J|A|C|S ARTICLES

Published on Web 12/18/2009

Oligomers of the Prion Protein Fragment 106−126 Are Likely Assembled from β-Hairpins in Solution, and Methionine Oxidation Inhibits Assembly without Altering the Peptide's Monomeric Conformation

Megan Grabenauer,[†] Chun Wu,[†] Patricia Soto,[†,‡] Joan-Emma Shea,[†,§] and Michael T. Bowers*,[†]

Departments of Chemistry and Biochemistry and of Physics, University of California, Santa Barbara, California 93106, and Department of Physics, Creighton University, Omaha, Nebraska 68178

Received July 7, 2009; E-mail: bowers@chem.ucsb.edu

Abstract: A portion of the prion protein, PrP106−126, is highly conserved among various species and is thought to be one of the key domains involving amyloid formation of the protein. We used ion mobility spectrometry−mass spectrometry (IMS−MS) in conjunction with replica exchange molecular dynamics (REMD) to examine the monomeric and oligomeric structures of normal PrP106−126 and two nonaggregating forms of the peptide, an oxidized form in which both methionine residues are oxidized to methionine sulfoxide and a control peptide consisting of the same amino acids as PrP106−126 in a scrambled sequence. Our ion mobility and simulation data indicate the presence of a population of β-hairpin monomers for the normal and oxidized peptides. This is supported by our CD data indicating that a monomer solution of the normal peptide contains ∼46% β-sheet and ∼23% β-turn content, in excellent agreement with our REMD simulations. Oligomerization was seen by IMS−MS for the normal peptide only, not the oxidized peptide or the control sequence. Both our IMS−MS and CD data suggest that this oligomerization results from the association of ordered β-hairpin monomers rather than disordered monomers. Structural analysis shows that the normal and oxidized peptides have similar secondary and tertiary structural properties, suggesting that the inhibition of aggregation caused by methionine oxidation stems from mediating interpeptide interactions rather than by altering the peptide's monomeric conformation. In contrast, an increase in α-helical and random coil structural components relative to the normal peptide might be responsible for the lack of observed aggregation of the control peptide.

Transmissible spongiform encephalopathies (TSEs) are a family of diseases that infect many species including humans (Creutzfeldt−Jakob disease, CJD, and Gerstmann−Straussler−Scheinker disease, GSS), sheep and goats (scrapie), cattle (bovine spongiform encephalopathy, BSE), and deer and elk (chronic wasting disease, CWD). These diseases are all characterized by the accumulation of an abnormally folded form of the prion protein as β-sheet-rich amyloid fibrils in the brain.[1] This abnormally folded form of the prion protein, PrP^{Sc}, has significantly more β-sheet and less α-helical content than the normal cellular form, PrP^{C}.[2] It remains under debate when and how monomers of PrP^{C} assemble into β-sheets. A popular belief is that ordered β-sheets are formed through a conformation transition of disordered aggregates to β-structure after initial nucleation.[3] Alternatively, it has been suggested that early ordered oligomers are nucleated from β-structure-rich monomers rather than unstructured coils. This idea is supported by theoretical studies showing that a fragment of the amyloid-β peptide can adopt a β-hairpin-like fold in monomers and small oligomers.[4,5] The latter mechanism appears physically attractive since it does not involve a drastic structural transition that is energetically unfavorable (rearrangement of large disordered aggregates at a late stage of amyloid fibril formation must involve overcoming a significant free energy barrier), but it has not been experimentally verified in any system.

Methionine oxidation appears to be a common factor affecting fibril formation in amyloid diseases[6] and has been shown to inhibit the pathogenic aggregation of amyloid-β,[7] PrP,[8] transthyretin,[9] and α-synuclein.[10] The inhibition might be caused by (A) a change of interpeptide interactions upon oxidation or

[†] Department of Chemistry and Biochemistry, University of California.
[‡] Creighton University.
[§] Department of Physics, University of California.

(1) Prusiner, S. B. *Science* **1991**, *252*, 1515–1522.
(2) Pan, K. M.; Baldwin, M.; Nguyen, J.; Gasset, M.; Serban, A.; Groth, D.; Mehlhorn, I.; Huang, Z. W.; Fletterick, R. J.; Cohen, F. E.; Prusiner, S. B. *Proc. Natl. Acad. Sci. U.S.A.* **1993**, *90*, 10962–10966.
(3) Chiti, F.; Dobson, C. M. *Annu. Rev. Biochem.* **2006**, *75*, 333–366.
(4) Baumketner, A.; Shea, J. E. *J. Mol. Biol.* **2006**, *362*, 567–579.
(5) Jang, S.; Shin, S. *J. Phys. Chem. B* **2006**, *110*, 19551958. Jang, S.; Shin, S. *J. Phys. Chem. B* **2008**, *112*, 3479–3484.
(6) Butterfield, D. A.; Kanski, J. *Mech. Ageing Dev.* **2001**, *122*, 945–962.
(7) Hou, L. M.; Kang, I.; Marchant, R. E.; Zagorski, M. G. *J. Biol. Chem.* **2002**, *277*, 40173–40176.
(8) Breydo, L.; Bocharova, O. V.; Makarava, N.; Salnikov, V. V.; Anderson, M.; Baskakov, I. V. *Biochemistry* **2005**, *44*, 15534–15543.
(9) Maleknia, S. D.; Reixach, N.; Buxbaum, J. N *FEBS J.* **2006**, *273*, 5400–5406.

10.1021/ja905595k

(B) a change of intrapeptide interactions upon oxidation, leading to a conformation change of the peptide monomer. Again, a definitive answer is impeded by a lack of detailed information on the structures of monomers and early oligomerization states of normal and oxidized peptides. Binger et al.[11] made a series of single and double methionine−glutamine substitutions on human apolipoprotein C-II (an amyloid fibril forming protein containing two methionines) to mimic the effect of oxidation and found no significant difference in the secondary structure between the wild type and glutamine-substituted mutants. Therefore, their data support mechanism A. However, since glutamine is not identical to an oxidized methionine and the same secondary structure could have a quite different tertiary structure, a direct study on the effects of oxidation at an atomic level is necessary. To address this issue, we used a combined experimental and theoretical approach to study monomer structures of a key fragment of PrP and its early oligomerization process.

A portion of the protein, PrP106−126, corresponding to residues 106−126 of the human PrP sequence (K^{106}TNMKHMAGAAAAGAVVGGLG^{126}), is highly conserved among various species and is thought to be one of the key domains involved in amyloid formation and the conformational change from the normal cellular form of the protein, PrP^{C}, to the β-sheet rich form, PrP^{Sc}.[12] The synthetic PrP106−126 peptide shares many similarities with PrP^{Sc}; it is highly amyloidogenic,[13] protease resistant,[13,14] and neurotoxic both in vivo[15,16] and in vitro.[16,17] Similarly to PrP^{Sc}, the neurotoxicity of this peptide requires the expression of PrP^{C},[18] providing a strong indication that the toxicity of this fragment reflects the pathogenic mechanism of PrP^{Sc}. Oxidation of the two methionine residues (Met^{109} and Met^{112}) has been shown to inhibit PrP106−126 aggregation.[17,19,20] In the work presented here, we examine an oxidized version of the peptide in which both methionine residues are intentionally converted to methionine sulfoxide to determine how this modification alters the monomeric structure of the peptide and its early oligomerization.

Although the monomeric form of PrP106−126 has been studied extensively by ensemble-averaging methods,[17,21−23] detailed molecular structures are not available due to the remarkable conformational polymorphism of this disordered peptide in solution. In addition, structural information about PrP106−126 has been notoriously difficult to obtain because of its aggregating nature and tendency to form complex fibrils having noncrystalline polymeric structures that are difficult to characterize using X-ray crystallography. Most of the structural information obtained so far has come from studies using CD[17,21] and NMR,[23,24] both of which reveal properties of the bulk solution, which may contain multiple oligomeric and conformational states. In this study we use the experimental technique of ion mobility spectrometry−mass spectrometry (IMS−MS)[25] in conjunction with molecular modeling to examine the conformations of this peptide. Unlike CD and NMR, IMS−MS allows us to selectively examine oligomeric states and/or conformational families. This technique is even more powerful when combined with state-of-the-art replica exchange molecular dynamics (REMD) simulations,[26,27] which yield information about structure at the atomic level.[28] In addition, CD is used to verify our REMD secondary structure population predictions, and AFM is used to verify the solution conditions for fibril formation.

Materials and Methods

Sample Preparation. PrP106−126 (KTNMKHMAGAAAAGAVVGGLG) was purchased from Bachem (Torrance, CA). An oxidized version in which both methionine residues were intentionally converted to methionine sulfoxide and a control peptide consisting of the same amino acids as PrP106−126 in a scrambled sequence (LVGAHAGKMGANTAKAGAMVG) were synthesized using solid-phase synthesis techniques and generously provided by Dr. Peter Heegaard. All peptides examined in this study had free N and C termini. Concentrated stock solutions were prepared by dissolving the lyophilized peptides in HPLC grade water (J.T. Baker, Phillipsburg, NJ) that was previously adjusted to pH 7 with dilute ammonium hydroxide and filtered through a 0.2 μm filter. Stock solutions were desalted using G-10 MacroSpin columns (Nest Group, Southborough, MA) and stored at −20 °C for later use. The resulting peptide samples had pH values between 6.8 and 7.0. Fresh samples of peptide in filtered HPLC grade water (20 μM for IMS−MS experiments and 100 μM for CD experiments) were prepared from the stock solutions immediately prior to use. The samples were left at room temperature for incubation studies.

(10) Uversky, V. N.; Yamin, G.; Souillac, P. O.; Goers, J.; Glaser, C. B.; Fink, A. L. *FEBS Lett.* **2002**, *517*, 239–244.
(11) Binger, K. J.; Griffin, M. D. W.; Howlett, G. J. *Biochemistry* **2008**, *47*, 10208–10217.
(12) Muramoto, T.; DeArmond, S. J.; Scott, M.; Telling, G. C.; Cohen, F. E.; Prusiner, S. B. *Nat. Med.* **1997**, *3*, 750–755. Muramoto, T.; Scott, M.; Cohen, F. E.; Prusiner, S. B. *Proc. Natl. Acad. Sci. U.S.A.* **1996**, *93*, 15457–15462. Brown, D. R.; Schmidt, B.; Kretzschmar, H. A. *Nature* **1996**, *380*, 345–347. Fischer, M.; Rulicke, T.; Raeber, A.; Sailer, A.; Moser, M.; Oesch, B.; Brandner, S.; Aguzzi, A.; Weissmann, C. *EMBO J.* **1996**, *15*, 1255–1264.
(13) Tagliavini, F.; Prelli, F.; Verga, L.; Giaccone, G.; Sarma, R.; Gorevic, P.; Ghetti, B.; Passerini, F.; Ghibaudi, E.; Forloni, G.; Salmona, M.; Bugiani, O.; Frangione, B. *Proc. Natl. Acad. Sci. U.S.A.* **1993**, *90*, 9678–9682.
(14) Forloni, G.; Angeretti, N.; Chiesa, R.; Monzani, E.; Salmona, M.; Bugiani, O.; Tagliavini, F. *Nature* **1993**, *362*, 543–546.
(15) Ettaiche, M.; Pichot, R.; Vincent, J. P.; Chabry, J. *J. Biol. Chem.* **2000**, *275*, 36487–36490.
(16) Chabry, J.; Ratsimanohatra, C.; Sponne, I.; Elena, P. P.; Vincent, J. P.; Pillot, T. *J. Neurosci.* **2003**, *23*, 462–469.
(17) Salmona, M.; Malesani, P.; De Gioia, L.; Gorla, S.; Bruschi, M.; Molinari, A.; Della Vedova, F.; Pedrotti, B.; Marrari, M. A.; Awan, T.; Bugiani, O.; Forloni, G.; Tagliavini, F. *Biochem. J.* **1999**, *342*, 207–214.
(18) Hope, J.; Shearman, M. S.; Baxter, H. C.; Chong, A.; Kelly, S. M.; Price, N. C. *Neurodegeneration* **1996**, *5*, 1–11. Brown, D. R.; Herms, J.; Kretzschmar, H. A. *NeuroReport* **1994**, *5*, 2057–2060.
(19) Heegaard, P. M. H.; Pedersen, H. G.; Flink, J.; Boas, U. *FEBS Lett.* **2004**, *577*, 127–133.
(20) Bergstrom, A. L.; Cordes, H.; Zsurger, N.; Heegaard, P. M. H.; Laursen, H.; Chabry, J. *J. Biol. Chem.* **2005**, *280*, 23114–23121.
(21) De Gioia, L.; Selvaggini, C.; Ghibaudi, E.; Diomede, L.; Bugiani, O.; Forloni, G.; Tagliavini, F.; Salmona, M. *J. Biol. Chem.* **1994**, *269*, 7859–7862.
(22) Villa, A.; Mark, A. E.; Saracino, G. A. A.; Cosentino, U.; Pitea, D.; Moro, G.; Salmona, M. *J. Phys. Chem. B* **2006**, *110*, 1423–1428. Di Natale, G.; Impellizzeri, G.; Pappalardo, G. *Org. Biomol. Chem.* **2005**, *3*, 490–497.
(23) Ragg, E.; Tagliavini, F.; Malesani, P.; Monticelli, L.; Bugiani, O.; Forloni, G.; Salmona, M. *Eur. J. Biochem.* **1999**, *266*, 1192–1201.
(24) Kuwata, K.; Matumoto, T.; Cheng, H.; Nagayama, K.; James, T. L.; Roder, H. *Proc. Natl. Acad. Sci. U.S.A.* **2003**, *100*, 14790–14795.
(25) von Helden, G.; Hsu, M. T.; Gotts, N.; Bowers, M. T. *J. Phys. Chem.* **1993**, *97*, 8182–8192. Wyttenbach, T.; Bowers, M. T. Gas-Phase Conformations: The Ion Mobility/Ion Chromatography Method. In *Modern Mass Spectrometry*; Schalley, C. A., Ed.; Springer: Berlin, 2003; pp 207−232.
(26) Geyer, C. J. *Computing Science and Statistics: Proceedings of the 23rd Symposium on the Interface*; Springer-Verlag: New York, 1991; pp 156−163. Hukushima, K.; Nemoto, K. *J. Phys. Soc. Jpn.* **1996**, *65*, 1604–1608. Swendsen, R. H.; Wang, J. S. *Phys. Rev. Lett.* **1986**, *57*, 2607–2609.
(27) Sugita, Y.; Okamoto, Y. *Chem. Phys. Lett.* **1999**, *314*, 141–151.
(28) Baumketner, A.; Bernstein, S. L.; Wyttenbach, T.; Bitan, G.; Teplow, D. B.; Bowers, M. T.; Shea, J. E. *Protein Sci.* **2006**, *15*, 420–428.

Ion Mobility and Mass Spectrometry. Mass spectra and mobility data leading to experimental collision cross sections were obtained on a home-built nano electrospray ionization mass spectrometer. Details of the instrumentation have previously been published.[29] The instrument consists of an ionization source, an ion funnel, a drift cell, and a quadrupole mass filter. To obtain mass spectra, ions are generated in the source and pass through the instrument as a continuous beam before arriving at the detector. For mobility data, the ion beam is trapped in the ion funnel and pulsed into the drift cell filled with ~5 Torr of helium buffer gas. Once inside the cell ions are pulled through by a weak electric field, E, and experience frictional drag due to the buffer gas, very quickly reaching a constant drift velocity, v_D, proportional to E:

$$v_D = KE \tag{1}$$

where the proportionality constant K is the ion mobility.

After exiting the drift cell, ions pass through the quadrupole mass filter and are detected as a function of time, producing an arrival time distribution (ATD). An ion's arrival time, t_a, is related to the reduced ion mobility, K_0, by

$$t_d = t_a - t_0 = \frac{l^2 T_0}{K_0 P_0 T}\frac{P}{V} \tag{2}$$

where t_d is the amount of time the ion spends inside the drift cell, t_0 is the amount of time the ion spends outside the drift cell, l is the length of the drift cell, T is the temperature inside the drift cell, P is the pressure inside the drift cell, V is the voltage applied across the drift cell, and T_0 and P_0 are standard temperature and pressure, respectively. t_a is measured at a series of field strengths, and plotting t_a vs P/V for a given temperature yields a straight line with an intercept equal to t_0. K_0 can be obtained from the slope of the line, and through the use of kinetic theory, the ion's collision cross section, σ, can be calculated using the following equation:[30]

$$\sigma = 1.3\left(\frac{z^2 E^2 T}{\mu k_B P^2 N^2 l^2}\right)^{1/2}(t_A - t_0) \tag{3}$$

where z is the ion's charge, μ is the reduced mass of the colliding particles (ion + He), k_b is the Boltzmann constant, and N is the He number density at STP.

Circular Dichroism. Circular dichroism experiments were performed at room temperature on an AVIV 202 circular dichroism spectrophotometer using a 0.1 cm path length quartz cell. Results presented are the average of four scans taken at 0.5 nm increments with an averaging time of 2 s and a 1 nm bandwidth. All spectra are background subtracted and smoothed using the Savitsky−Colay method with a polynomial order of 3 and a smoothing window of 15 points.[31] Mean residue ellipticities were calculated using

$$[\theta] = \frac{\theta}{lCN_r} \tag{4}$$

where θ is the ellipticity in millidegrees, l is the path length in millimeters, C is the molar concentration of the peptide, and N_r is the number of residues. The secondary structure population was analyzed using the constrained least-squares fitting analysis program LINCOMB[32] with a polypeptide-based reference set.[33]

Molecular Dynamics Simulations. The AMBER 9[34] suite was used in REMD[27] simulations and data processing. All three peptides were modeled with a net charge of +2 and unblocked termini, using the AMBER all-atom point-charge force field, ff96.[35] Studies[36] have shown that ff96 combined with a recent generalized-born implicit solvent model (IGB=5)[37] plus the surface term (gbsa=1, surface tension=5.0 cal/mol/Å^2) predicts reasonable structures for small α, β, and α/β proteins, and ff96 is fairly well-balanced between α-helix and β-sheet. The parameters for a singly oxidized methionine residue were derived by following the same protocol used in developing AMBER ff96.

REMD simulations were used to generate two types of theoretical structures: solvent-free (preferred gas-phase conformations) and dehydrated solution (the result of removing water molecules from solution structures, mimicking transfer of the solution structure into a vacuum). Starting structures were created by building extended chain conformations and then subjecting them to an initial energy minimization. Solvent-free simulations were carried out in a vacuum, and solution-phase structures were generated using the implicit solvent model mentioned above to represent solvation effects with an effective salt concentration of 0.2 M. Sixteen replicas were set up with temperatures exponentially spaced from 270 to 465 K for solution-phase calculations (i.e., 270.0, 278.9, 289.3, 300.0, 311.2, 322.7, 334.7, 347.2, 360.1, 373.4, 387.3, 401.7, 416.6, 432.1, 448.2, and 465.0 K) and 300−2200 K for solvent-free calculations (i.e., 300.0, 342.6, 391.3, 446.9, 510.4, 582.8, 665.6, 760.2, 868.2, 991.5, 1132.4, 1293.2, 1476.9, 1686.7, 1926.4, and 2200.0 K). The temperature values were optimized using the algorithm described by Wu et al.[38] Extreme high temperature (i.e., up to 2200 K) was used in the solvent-free simulations to overcome slow structural relaxation and did not produce any notable structural artifacts (e.g., trans to cis isomerizations of peptide bonds) within the duration of the simulations (40.0 ns for each replica). Initial velocities of atoms for each replica were generated according to the Maxwell−Boltzmann distribution for that replica's initial temperature. The first 1.0 ns of molecular dynamics in each replica was performed without replica exchanges to equilibrate the system at its target temperature. After the first 1.0 ns, exchanges between neighboring replicas were attempted every 2000 MD steps (2.0 ps), and the exchange rate among replicas was ~20%. SHAKE[39] was applied to constrain all bonds connecting hydrogen atoms, and a shorter time step of 1.0 fs rather than the typical 2.0 fs was used to avoid the SHAKE failure associated with large atomic displacements at the high temperatures used in our simulations. To reduce the computation time, nonbonded forces were calculated using a two-stage RESPA approach[40] where the forces within a 12 Å radius were updated every step and those beyond 12 Å were updated every two steps. Temperature was controlled using Berendsen's algorithm[41] with a coupling constant of 1.0 ps. The center of mass translation and rotation were removed every 500 MD steps (0.5 ps). Each solution-phase replica was run for 200.0 ns, resulting in an aggregated simulation time of 3.2 μs for each peptide, and each solvent-free replica was run for 40.0 ns, resulting in an aggregated

(29) Wyttenbach, T.; Kemper, P. R.; Bowers, M. T. *Int. J. Mass Spectrom.* **2001**, *212*, 13–23.
(30) Mason, E. A.; McDaniel, E. W. *Transport Properties of Ions in Gases*; Wiley: New York, 1978.
(31) Greenfield, N. J. *Nat. Protoc.* **2006**, *1*, 2876–2890.
(32) Perczel, A.; Park, K.; Fasman, G. D. *Anal. Biochem.* **1992**, *203*, 83–93.
(33) Sreerama, N.; Woody, R. W. *Anal. Biochem.* **1993**, *209*, 32–44.
(34) Case, D. A.; et al. *AMBER 9*; University of California: San Francisco, 2006.
(35) Kollman, P.; Dixon, R.; Cornell, W.; Fox, T.; Chipot, C.; Pohorille, A. *Computer Simulation of Biomolecular Systems: Theoretical and Experimental Applications*; Kluwer: Dordrecht, 1997; pp 83−96.
(36) Ozkan, S. B.; Wu, G. A.; Chodera, J. D.; Dill, K. A. *Proc. Natl. Acad. Sci. U.S.A.* **2007**, *104*, 11987–11992. Shell, M. S.; Ritterson, R.; Dill, K. A. *J. Phys. Chem. B* **2008**, *112*, 6878–6886.
(37) Onufriev, A.; Bashford, D.; Case, D. A. *Proteins: Struct., Funct., Bioinf.* **2004**, *55*, 383–394.
(38) Wu, C.; Murray, M. M.; Bernstein, S. L.; Condron, M. M.; Bitan, G.; Shea, J.-E.; Bowers, M. T. *J. Mol. Biol.* **2009**, *387*, 492–501.
(39) Ryckaert, J. P.; Ciccotti, G.; Berendsen, H. J. C. *J. Comput. Phys.* **1977**, *23*, 327–341.
(40) Procacci, P.; Berne, B. J. *Mol. Phys.* **1994**, *83*, 255–272.
(41) Berendsen, H. J. C.; Postma, J. P. M.; van Gunsteren, W. F.; Dinola, A.; Haak, J. R. *J. Chem. Phys.* **1984**, *81*, 3684–3690.

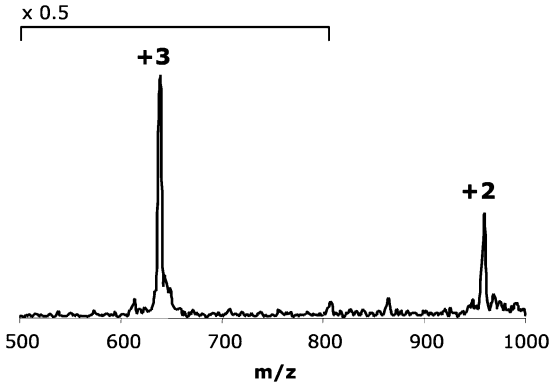

Figure 1. Mass spectrum of normal PrP106−126 in water. The +2 charge state has an *m/z* ratio of 957, and the +3 charge state has an *m/z* ratio of 638.

simulation time of 640.0 ns for each peptide. The replica trajectories were saved at 2.0 ps intervals for further analysis.

The STRIDE program of Frishman and Argos[42] was used for secondary structure assignment, and tertiary fold analysis was carried out using the GROMACS clustering protocol,[43] in which pairwise rmsd (root mean square deviation) over Cα atoms is used as a similarity metric to classify structural families. For each structural family, the centroid (the structure having the largest number of neighboring structures within the rmsd cutoff of 2.5 Å) was selected as the representative structure of that structural family. The structural families were further merged into a super structural family on the basis of fold topology. Collision cross sections of the representative structures were calculated using a trajectory method.[44] To better correlate with the solvent-free experiments, solution-phase structures were converted to "dehydrated" structures via an energy minimization (500 000 steps) in a vacuum prior to the cross section calculations. This generally reduces the overall size of the structure, while maintaining solution structure features.

REMD simulations were used to generate both solvent-free and solution-phase structures. Solvent-free structures were compared directly with experimental measurements, while solution-phase structures were converted to dehydrated solution structures prior to comparison with experiment. The convergence of the REMD simulations was rigorously verified by a block analysis. The total sampling times of 200.0 ns for the solvated and 40.0 ns for the solvent-free simulations at 300 K were equally divided into four blocks, and the secondary structure and tertiary structure clustering analyses detailed above were performed for each block. For all six sets of REMD simulations, good convergence was found during the last half of the simulations (see, for example, the data for the normal peptide of PrP106−126 in Figure S5 of the Supporting Information). The structural results presented in this paper were from the last half of the trajectory at 300 K (i.e., the last 100.0 ns of the solvated simulations and the last 20.0 ns of the solvent-free simulations).

Results

The mass spectrum of the normal peptide in water is shown in Figure 1. The spectrum consists of a peak at 957 *m/z* for the +2 charge state and a peak at 638 *m/z* for the +3 charge state. (A peak near 1912 *m/z* for the +1 charge state is not observed.) The +2 charge state corresponds to the native state of the peptide in which the two basic residues (K^{106} and K^{110}) and both the N and C termini are charged at the normal physiological condition (pH ≈ 7.0), whereas the +3 charge state likely results from protonation of the C-terminus during the electrospray ionization process in the experiment, and thus, it is not the main focus of this study. Mass spectra for the control peptide (see the Materials and Methods for the sequence) and the oxidized peptide are similar to that of the normal peptide in Figure 1 and are presented in Supporting Information Figure S1.

ATDs for the +2 charge state of the normal and oxidized peptides are very similar to each other and are dominated by a compact family of structures with a drift time near 470 μs (Figure 2A; see Supporting Information Figure S2 for +3 charge state data). Interestingly, a small amount of an extended family of structures is also present with a drift time near 560 μs. This extended structural family is seen only in the normal and oxidized peptide samples, always with low intensity, but never in control peptide samples. ^{13}C isotope distributions of each ATD component obtained on a modified Q-Tof instrument[45] (Supporting Information Figure S3) indicate that both of these features are due to monomeric forms of the peptides. ATDs for the control peptide contain a single compact family of structures. Cross sections of the compact structures of the normal and oxidized peptides are very similar, with the +2 charge state having an average cross section around 370 $Å^2$. The control peptide is somewhat larger, with the +2 charge state having an average cross section of 391 $Å^2$. The extended families of structures of the normal and oxidized PrP106−126 peptides also appear to be very similarly sized. Cross sections for each peptide are summarized in Table 1.

The ability of the normal peptide to form fibrils in filtered HPLC water was confirmed by atomic force microscopy (AFM) of an 800 μM sample incubated at 30 °C for three days (Supporting Information Figure S4). To study the early oligomerization behavior of these peptides, 20 μM samples were incubated at room temperature for 72 h and monitored by IMS−MS. The ATD of the +2 charge state of the normal peptide changes over time, while no changes are observed in ATDs of the control and oxidized peptides over the same time period (Figure 2). The +2 ATD for the fresh sample has a dominant feature at 470 μs with an average cross section of 371 $Å^2$ and a much weaker extended feature near 560 μs with an average cross section of 466 $Å^2$. After 24 h, Figure 2B, there is a substantial reduction in the extended structure at 560 μs and a new feature is evident as a shoulder, at shorter time, of the dominant peak, near 425 μs. By 72 h, Figure 2C, almost all of the extended structure is depleted and a second new feature has grown in near 390 μs. When the cross sections of these new features are calculated assuming they are compact conformers of the monomer +2 charge state, values of 347 and 302 $Å^2$ are obtained. The latter value is much smaller than those of any monomeric structures generated by theory (Supporting Information Figures S5 and S6). Consequently, the most probable explanation is that this is an oligomer. (Oligomers with the same *z/n* value, where *z* = charge and *n* = oligomer order, always appear at shorter drift times than the monomer.[46]) This oligomer is most likely dominantly formed from the extended

(42) Frishman, D.; Argos, P. *Proteins: Struct., Funct., Genet.* **1995**, *23*, 566–579.
(43) Daura, X.; Gademann, K.; Jaun, B.; Seebach, D.; van Gunsteren, W. F.; Mark, A. E. *Angew. Chem., Int. Ed.* **1999**, *38*, 236–240.
(44) Mesleh, M. F.; Hunter, J. M.; Shvartsburg, A. A.; Schatz, G. C.; Jarrold, M. F. *J. Phys. Chem.* **1996**, *100*, 1608216086. Shvartsburg, A. A.; Jarrold, M. F. *Chem. Phys. Lett.* **1996**, *261*, 86–91.
(45) Pringle, S. D.; Giles, K.; Wildgoose, J. L.; Williams, J. P.; Slade, S. E.; Thalassinos, K.; Bateman, R. H.; Bowers, M. T.; Scrivens, J. H. *Int. J. Mass Spectrom.* **2007**, *261*, 1–12.
(46) Bernstein, S. L.; Wyttenbach, T.; Baumketner, A.; Shea, J. E.; Bitan, G.; Teplow, D. B.; Bowers, M. T. *J. Am. Chem. Soc.* **2005**, *127*, 2075–2084.

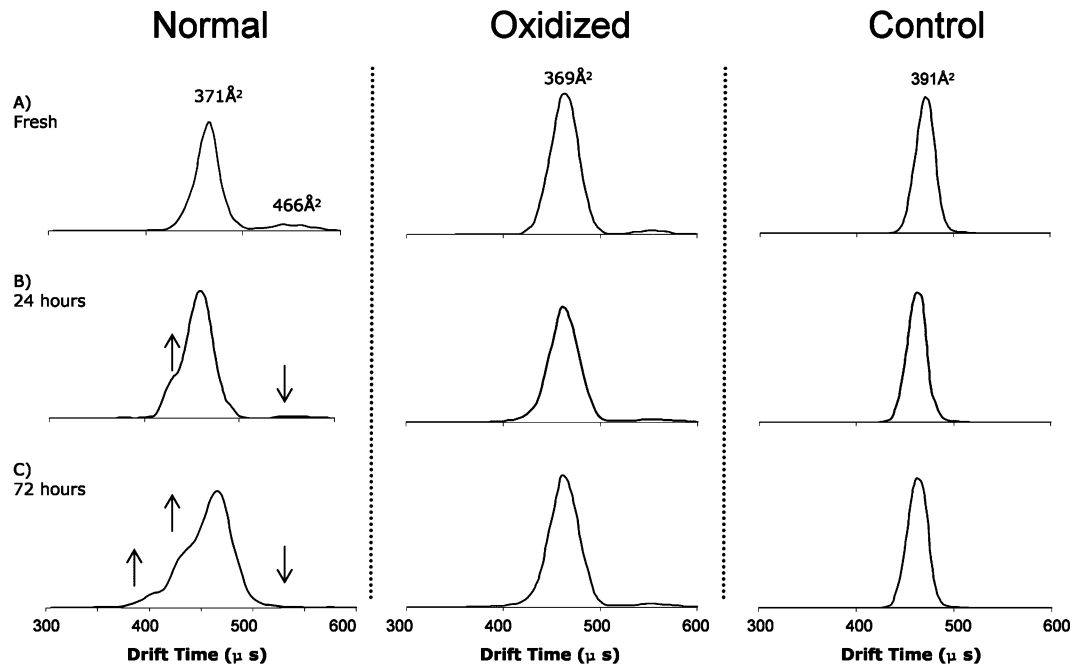

Figure 2. ATDs of the +2 charge state of the normal, oxidized, and control peptides in water: A, fresh; B, after 24 h at room temperature; C, after 72 h at room temperature. After 72 h two new features are present in the ATD for the normal peptide, most likely due to oligomer formation (see the text). While the putative oligomeric features emerge, the extended monomer feature disappears.

Table 1. Summary of Experimental Cross Sections (Å²) of the Peptides[a]

	+2 charge state		+3 charge state	
peptide	compact	extended	compact	extended
normal	371	466	390	–
oxidized	369	460	383	–
control	391	–	406	–

[a] Experimental cross sections were reproducible to within 3%.

monomers, as suggested by the concurrent depletion of the extended feature in the ATD with the appearance of the early arrival time features.

The peak at 425 μs with a cross section of 347 Å^2 is either a new compact conformer of the monomer or an oligomer. If it is a monomer, it must be slowly formed in solution and then sprayed into the gas phase where it is detected. This is extremely unlikely from a kinetic point of view as the stable solution conformers should be essentially instantaneously formed upon dissolution of the peptide in water and relatively rapidly come into equilibrium. Furthermore, it would have to be a solution conformer that is more compact than the most compact solvent-free conformer. The most compact family of solution structures predicted by the REMD modeling has an average cross section of ~425 Å^2. Even if this new monomer conformer appeared in solution and converted to a "new" gas-phase conformer, it would still be more compact than the most compact solvent-free conformer predicted by the REMD calculations (~360 Å^2). Finally, the REMD calculations yield essentially the same families of monomer structures for both the native and oxidized peptides. This new feature does not appear in the experimental ATD of the oxidized peptide, only in the normal ATD, suggesting it is not a monomer feature.

On the other hand, it is reasonable that an oligomer would appear over time in a solution of a known aggregating peptide. If this is a dimer, then the cross section is 694 Å^2, which is about the right degree of accommodation expected for a peptide of this size (dimers are always smaller than two monomers due to the contact surface they share). A dimer is reasonable for this species as aggregation in all known systems starts with dimerization. The second peak at 390 μs could then reasonably be either a trimer or a tetramer. Detailed modeling or the ability to detect ^{13}C isotope separations would be needed to pin down the assignment and to prove the 425 μs peak is indeed a dimer.

The modified Q-Tof instrument used to measure ^{13}C isotope distributions has a homemade off-axis nanospray source that has been observed to be relatively harsh (high collision energy). As a result, no evidence for oligomerization of the incubated samples was seen on that instrument, most likely due to oligomer dissociation before mass spectra could be obtained. Hence, definitive orders of the oligomers could not be determined. No change in the ATDs of the oxidized samples was observed over the 72 h incubation, in agreement with other experiments[17,19,20] showing that methionine oxidation inhibits aggregation.

The fact that evidence for oligomerization is seen in ATDs but not in mass spectra is not necessarily surprising. This could be due to oligomerization to masses outside the limited mass range of our instrument (as observed in α-synuclein/spermine aggregation[47]) or to a preference for formation of like-charged oligomers (as observed in the Aβ peptide[48]). Unambiguous oligomer peaks must have *z/n* values that do not overlap with monomer *z/n* values, and with limited places to put a charge on such a small peptide, it is possible that such distinct *z/n* peaks do not occur. In addition, the pulsed nature of data collection for ATDs is much more sensitive than the scanning mode used for mass spectra, allowing detection of small population changes in solution.

(47) Grabenauer, M.; Bernstein, S. L.; Lee, J. C.; Wyttenbach, T.; Dupuis, N. F.; Gray, H. B.; Winkler, J. R.; Bowers, M. T. *J. Phys. Chem. B* **2008**, *112*, 11147–11154.
(48) Bernstein, S. L.; Dupuis, N. F.; Lazo, N. D.; Wyttenbach, T.; Condron, M. M.; Bitan, G.; Teplow, D. B.; Shea, J.-E.; Ruotolo, B. T.; Robinson, C. V.; Bowers, M. T. *Nat. Chem.* **2009**, *1*, 326–331.

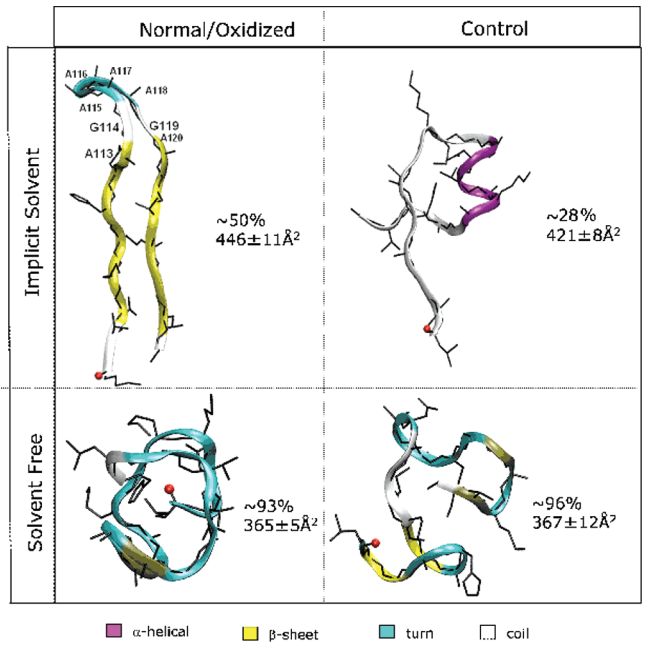

Figure 3. Representative peptide structure of a supercluster for each peptide from the REMD simulations in implicit solvent and under solvent-free conditions at 300 K. The percentage of the population contained within the top three clusters (see Figures S5 and S6 of the Supporting Information for the structures) and average collision cross sections for each simulation are shown below the structures. α-Helical, β-sheet, turn, and coiled conformations are colored in purple, yellow, cyan, and white, respectively.

To explore the structural features linked to the aggregation of PrP106−126, molecular modeling was focused on the +2 charge states of the peptides, as that is the expected charge state of the peptide in physiological solution conditions and it was the only charge state for which evidence of aggregation was seen experimentally. Calculated cross sections and representative structures of super structural families from the simulations done in implicit solvent and under solvent-free conditions are shown in Figure 3 (the structural families in each superfamily are shown in Figures S5 and S6 of the Supporting Information). Solvent-free structures are smaller than solution-phase structures due to elevated electrostatic interactions in a vacuum (e.g., the dielectric constant decreases to 1 in a vacuum from 78.5 in water solvent).

For the normal and oxidized peptides, simulations carried out under solvent-free conditions produced structures with calculated cross sections in good agreement with those of the compact families of structures seen experimentally. Simulations in implicit solvent produced more extended structures (β-hairpin) with larger cross sections more comparable to those of the extended features seen in the ion mobility experiments. Consequently, we assign the compact structures seen in the ATDs for the normal and oxidized peptides as solvent-free structures that retain little to none of their original solution structural properties, while the larger families are dehydrated solution structures of β-hairpin. This shift to gas-phase structure is not unexpected as it has previously been shown that for some small peptides[38] and DNA systems[49] a significant loss of solution structure occurs upon transfer to the gas phase. ATDs for the control peptide show only one, relatively compact, family of structures and on the basis of only comparison to the simulation data, it is unclear whether they are solvent-free or solution-phase structures. The experimental cross section (391 Å^2) falls between cross sections predicted from simulations for solvent-free (367 ± 12 Å^2) and implicit solvent (421 ± 8 Å^2) structures. However, the experimental value is closer to that of the solvent-free structures than that of the implicit solvent structures.

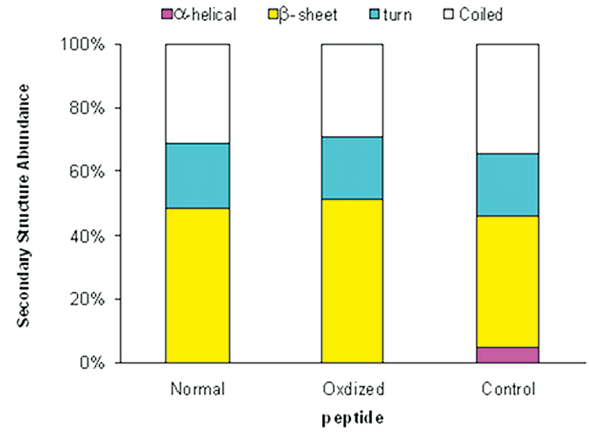

Figure 4. Secondary structure abundance averaged from the equilibrium ensemble (last 100 ns) at 300 K from the REMD simulations in implicit solvent for the normal, oxidized, and control peptides of PrP106−126 in the +2 charge state with unblocked termini. The mean standard error is ~1%, estimated from the block analysis.

Since aggregation occurring in solution is most relevant to biological systems, structure analysis was focused on the solution simulations. The secondary structure propensities of each of the three peptides at 300 K are summarized in Figure 4. The normal and oxidized peptides have very similar secondary structure propensities of ~50% β-sheet, ~30% coil, ~20% turn, and no α-helix. These two peptides adopt a β-hairpin-like fold. Stabilizing forces for the β-hairpin include main-chain hydrogen bonds, van der Waals interactions, hydrophobic interactions between the four alanine residues in the turn region (Ala^{114}-Ala^{115}-Ala^{116}-Ala^{117}), hydrophobic interactions between two alanine residues on opposite sides of the hairpin (Aal^{113}-Ala^{120}), and, in the normal peptide, hydrophobic interactions involving the two methionine residues (Met^{109}-Leu^{125}, Met^{112}-Val^{12}). The secondary structure of the control sequence is significantly different from that of the other two peptides, having a reduced β-conformation propensity (40% vs ~50%), an increased α-helical conformation propensity (5% vs 0%), a slightly increased coiled conformation propensity (34% vs ~30%), and a similar turn conformation propensity (20% vs 20%). Overall, the control sequence adopts a compact globular conformation.

To verify our REMD secondary structure predictions, we measured the CD spectrum of the normal peptide in water (Figure 5). To ensure a monomer-dominant solution, a 100 μM solution, the lowest peptide concentration allowed by the sensitivity of the CD instrument, was prepared immediately prior to analysis. The populations of secondary structures obtained from the CD data of the fresh solution are in excellent agreement with our REMD-predicted values (Table 2). Over the course of a 26 day room temperature incubation the β-sheet and β-turn populations increased slightly from ~46% and ~23% to ~52% and ~27%, respectively. We expect that after the 26 day incubation some of the peptide was oligomerized, due to the higher concentration (100 μM) and longer incubation time of this sample compared to the IMS−MS sample (20 μM) that was found to form oligomers after 3 days. Examination by AFM did not reveal any fibrils however, indicating that the sample was still in the early stages of aggregation. Therefore, the

(49) Baker, E. S.; Bowers, M. T. *J. Am. Soc. Mass Spectrom.* **2007**, *18*, 1188–1195.

Table 2. Secondary Structure of PrP106−126 in Water from the CD Experiment and the REMD Simulation[a]

	secondary structure population (%)			
	α-helix	β-sheet	β-turn	coil
fresh solution (water solvent)	0 ± 0.2	46 ± 1.0	23 ± 0.3	31 ± 0.5
incubated for 26 days	0 ± 0.2	52 ± 1.1	27 ± 1.0	21 ± 0.5
REMD simulation	0 ± 0.3	48 ± 5.0	20 ± 0.1	32 ± 0.3

[a] The error for REMD simulation is estimated from the block analysis (Figure S7, Supporting Information).

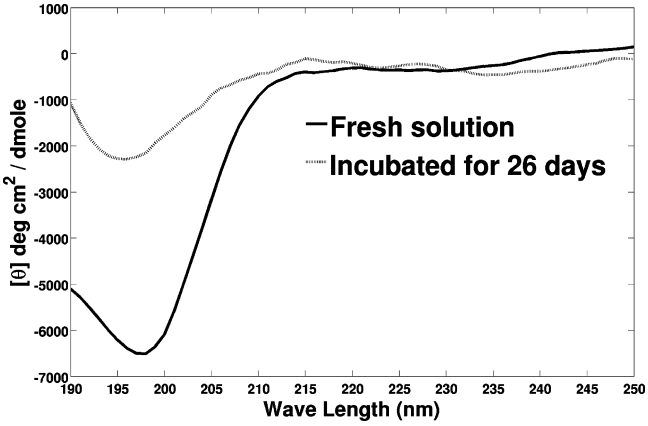

Figure 5. CD spectra of normal PrP106−126 in water at room temperature.

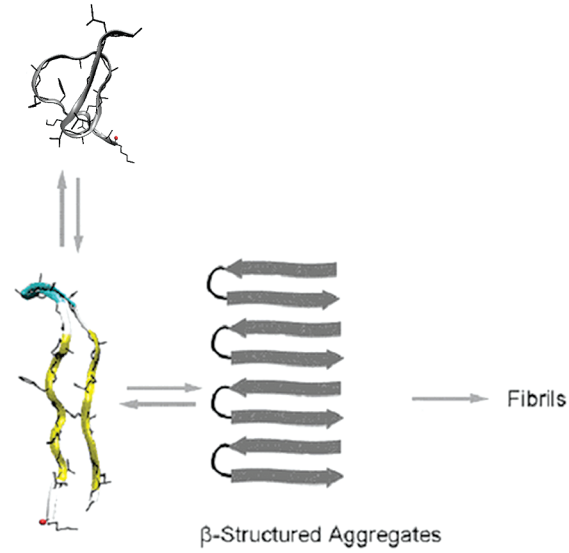

Figure 6. Proposed mechanism of PrP106−126 oligomer formation involving the assembly of ordered β-hairpin monomers, rather than disordered monomers, to form ordered small aggregates.

increase of β-content over time suggests that these early oligomers have a high β-content, further supporting our proposal that the early oligomers are formed from the association of β-hairpins.

For the normal and oxidized peptides, the abundance of β-hairpin seen in the IMS−MS experiments (~5%, estimated from the area of the extended feature shown in the ATD in Figure 2A) is much lower than the ~50% abundance seen in the simulations and in a circular dichroism spectrum of the normal peptide in water, Figure 5 and Table 2. This difference is most likely caused by the conversion of β-hairpin to a more compact structure following solvent evaporation.

Discussion

PrP106−126 is an amyloidogenic peptide that is neurotoxic in vivo.[15,16] Whereas the final products of the pathogenic aggregation are well characterized as β-sheet-rich amyloid fibrils, the structures of peptide monomers and early oligomerization states are poorly understood. It is generally believed that highly ordered β-sheets are formed late in the aggregation process from the association of disordered monomers and small aggregates, through a conformation transition to β-structure after fibril nucleation.[3] This belief is reinforced by a lack of well-defined monomeric β-structure for amyloid peptides in solution as determined from CD and NMR. However, these techniques only reveal properties of the bulk solution and are limited to being able to measure average structures in such solutions. Theoretical studies have shown that a fragment of the amyloid-β peptide can adopt a β-hairpin-like fold in monomers and small oligomers,[4,5] suggesting that early ordered oligomers are nucleated from β-structure-rich monomers rather than unstructured coils. (We will refer to this as the "early conformation transition" mechanism.) This mechanism appears physically attractive since it does not involve a drastic structural transition after nucleation that is energetically unfavorable (rearrangement of large disordered aggregates at a late stage of amyloid fibril formation must involve a significant free energy barrier), but it has not been widely studied. Our observations of monomeric β-hairpin structure by IMS−MS and REMD and the formation of early oligomers that correlate with loss of β-hairpin monomers provide support for the early conformation transition mechanism, shown schematically in Figure 6. Our CD data confirm the secondary structure predictions from REMD simulations, also supporting the early conformation transition by showing that early oligomerization of the peptide coincides with an increase in β-structural content.

In this study, oligomerization was seen in the normal peptide only, not in the oxidized version or the control sequence. Oligomerization of the normal peptide was very reproducible under the conditions used in this study, with the appearance of the same new oligomeric features and simultaneous disappearance of the extended features seen in ATDs taken from samples in water after 24 and 72 h at room temperature across multiple trials. These data strongly suggest that the new oligomers are formed from monomers having an extended conformation. Our simulation data further suggest that the extended feature in the ATDs corresponds to β-hairpin. In contrast, the ATDs for the two nonaggregating forms of the peptide (the oxidized version and the control peptide) did not change over the same time period.

Previous studies have shown that methionine oxidation inhibits the aggregation of PrP106−126.[19,20] Our results are consistent with the results of these studies. In contrast to the changes observed in the ATD of the +2 charge state of the normal peptide, the ATD for the +2 charge state of the oxidized peptide remains unchanged after 72 h of incubation, indicating no oligomerization of the oxidized peptide. Our experimental and simulation data both suggest the monomeric forms of the

two peptides have very similar secondary and tertiary structural properties. Therefore, the oxidation does not significantly change the monomer structure, and the effect of the methionine oxidation on reducing the aggregation propensity most likely stems from reducing the hydrophobic interactions for interpeptide association by converting the hydrophobic methionine side chain to hydrophilic sulfoxide upon oxidation. In particular, without the extra hydrophobic interactions (Met^{109}-Leu^{125} and Met^{112}-Val^{121}), the β-hairpin of the oxidized peptide may be less likely to form a long β-sheet. To the best of our knowledge, our present work provides the first direct evidence of this inhibition mechanism due to methionine oxidation, which has previously been proposed by Binger et al.[11] on the basis of their methionine−glutamine substitution study on human apolipoprotein C-II. This mechanism should also be applicable to other amyloid peptides having methionine residues.

The normal and oxidized peptides adopt a β-hairpin-like fold that is stabilized by multiple hydrophobic interactions along with main chain hydrogen bonds and van der Waals interactions. The hydrophobic interactions are critical for stabilizing the β-hairpin structure, as indicated by a reduction of the β-hairpin population when solvent water molecules are removed from the peptides (Figure 2). These intrapeptide hydrophobic clusters are also expected to play an important role in interpeptide interactions for forming long β-sheets and eventually amyloid fibrils. In addition, the turn region of these β-hairpins is centered near the palindromic portion of the sequence, AGAAAAGA. Modifications in this region have been shown to have dramatic effects on the neurotoxicity and secondary structure properties of PrP106−126,[50] possibly because an interruption in this portion of the sequence may prevent the formation of a hairpin-like fold. Intriguingly, the β-hairpin-like fold is seen in fragments of the amyloid-β peptide[4,51] responsible for Alzheimer's disease and has very recently been identified in the islet amyloid polypeptide (IAPP) responsible for diabetes type II.[52]

The control peptide has quite different secondary and tertiary structural properties compared to the normal and oxidized peptides. The control peptide has less β-sheet than the normal peptide and greater α-helical and random coil structural components. Unlike oxidation, which appears to inhibit aggregation by mediating interpeptide interactions, these structural differences at the monomeric level are most likely responsible for the lack of observed aggregation of the control peptide.

Acknowledgment. We thankfully acknowledge Dr. Peter Heegaard for supplying the PrP106−126 samples. The support of the Department of Environment Food and Rural Affairs, U.K. (M.T.B.), the David and Lucile Packard Foundation (J.-E.S.), and National Science Foundation Grants CHE-0909743 (M.T.B.) and MCB-0642088 (J.-E.S.) is gratefully acknowledged. Simulations were performed on the Lonestar cluster at the Texas Advanced Computing Center (Grant LRAC MCA05S027 to J.-E.S.). This work made use of MRL Central Facilities supported by the MRSEC Program of the National Science Foundation under Award No. DMR05-20415.

Supporting Information Available: Mass spectra of control and oxidized peptides, ATD comparison of the oxidized peak in the normal sample and the oxidized sample, ATD data for the +3 charge state of all peptides, ^{13}C isotope distributions of the two features in the normal sample +2 charge state ATD, AFM image of PrP106−126 fibrils, representative structures, relative abundances, and cross sections of the top three clusters from the REMD simulations in vacuum and implicit solvent, convergence check of the REMD simulations, and complete ref 34. This material is available free of charge via the Internet at http://pubs.acs.org.

JA905595K

(50) Jobling, M. F.; Stewart, L. R.; White, A. R.; McLean, C.; Friedhuber, A.; Maher, F.; Beyreuther, K.; Masters, C. L.; Barrow, C. J.; Collins, S. J.; Cappai, R. *J. Neurochem.* **1999**, *73*, 1557–1565. Brown, D. R. *Mol. Cell. Neurosci.* **2000**, *15*, 66–78.
(51) Han, W.; Wu, Y. D. *J. Am. Chem. Soc.* **2005**, *127*, 15408–15416.
(52) Dupuis, N. F.; Wu, C.; Shea, J.-E.; Bowers, M. T. *J. Am. Chem. Soc.*, in press.